Li 2 TiO 3 /Graphene and Li 2 TiO 3 /CNT Composites as Anodes for High Power Li-Ion Batteries

Ambadi Lakshmi-Narayana, Merum Dhananjaya, Nunna Guru-Prakash, Obili M Hussain, Alain Mauger, Christian M Julien

Li_2TiO_3/graphene and Li_2TiO_3/CNT composites as anodes for high power Li-ion batteries

A. Lakshmi-Narayana[a], M. Dhananjaya [a], N. Guru-Prakash[a], O. M. Hussain[a,*],

A. Mauger[b], and C. M. Julien[b]

[a] Thin Films Laboratory, Department of Physics, Sri Venkateswara University, Tirupati-517502, India.

[b] Sorbonne Université, UPMC Univ Paris 06, Institut de Minéralogie, de Physique des Matériaux et de Cosmochimie (IMPMC), CNRS UMR 7590, 4 place Jussieu, 75005 Paris, France

Corresponding author: C.M. Julien, e-mail:christian.julien@upmc.fr

Abstract

Three-dimensional composites Li_2TiO_3/graphene (LTO/Gr) and Li_2TiO_3/carbon nanotube (LTO/CNTs) were synthesized by solid-state reaction for application as anode materials for lithium-ion batteries. These composites are structurally characterized by X-ray diffraction, Raman spectroscopy and high-resolution transmission electron microscopy, while electrochemically tests are performed by cyclic voltammetry and chronopotentiometry. The synergetic effect of graphene and CNTs with LTO facilitate the network conduction leading to faster electron and Li^+ ion transfer and improve cycling stability and rate capability of the anode. The LTO/Gr and LTO/CNTs composites exhibited an initial discharge capacity as high as 154 and 149 mAh g^{-1} at 1C rate, respectively and retained excellent cycling stability of 98% and 96% after 30 charge–discharge cycles.

Keywords: solid state reaction; Li_2TiO_3/graphene; Li_2TiO_3/CNT; composite anodes; electrochemical performance.

Introduction

Lithium-ion batteries (LIBs) have been considered as one of the promising technologies for next generation plug-in hybrid electric vehicles (HEV), electric vehicles (EV) and stationary power storage due to the merits of high-energy density, high voltage, small self-discharge and light weight.[1,2] In commercial LIBs, lithiated metal oxides and carbonaceous materials are commonly employed as positive and negative electrode materials, which are active elements determining the energy and power densities. However, carbon-based anodes suffer from formation of solid-electrolyte interface (SEI). Since the SEI is resistive, it may generate heat during operation and cause fire with the presence of carbonates in electrolyte.[3] Among alternative anode materials, lithium titanate $Li_4Ti_5O_{12}$ has attracted much attention, because of its reversible lithium-ion insertion and extraction reaction due to its zero-strain properties during charge/discharge process.[4] Another titanate Li_2TiO_3 (denoted LTO hereafter) is also a possible zero-strain anode material in LIBs but is hampered by unsatisfactory rate capability due to kinetic issues associated with poor electrical conductivity ($\sigma_e=10^{-11}$ S cm^{-1}) and initial capacity loss.[5-7] Thus far, several effective approaches have shown to improve σ_e of titanate materials such as doping with metallic or non–metallic ions,[8] reduction of particle size to nanoscale, deposition of a thin layer (coating) on the particle surface,[9] and/or fabrication of composite material.[10] The drawback of doping atoms is a decrease of the amount of active Ti^{4+} ions, and thus a decrease of the capacity of the titanate anode.[11] Reduction of the size of the particles to the nano-range is expected to enhance the capacity and rate capability owing to the reduction of the length of the path that ions and electrons have to travel to reach the surface of the particles.[12] However, the inherent disadvantage is the agglomeration of primary particles limiting their uniform dispersion in the electrode. In addition, nanocomposites made of metal oxides with carbonaceous materials have enhanced electrochemical properties owing to improved electric conductivity and morphological stability.[13,14] Furthermore, the dispersion of metal oxides with the carbon material hinders the agglomeration of particles providing efficient and stable framework during charge/discharge cycling. Noteworthy, the rate capability of $Li_4Ti_5O_{12}$ and Li_2TiO_3 has been significantly improved by forming nanocomposites by various synthesis methods. Carbon based materials such as carbon nanotubes (CNTs), reduced graphene oxide (rGO) and graphene were used in the

preparation of such nanocomposites with $Li_4Ti_5O_{12}$.[15,16] Graphene (Gr) and rGO are the most conductive forms of carbon and thus a usual additive to increase the C-rate of any lithium-based battery. To our knowledge, however, Li_2TiO_3 mixed with acetylene black has been tested recently as an anode, but not Li_2TiO_3/CNTs, Li_2TiO_3/Gr composites, which is the purpose of the present work.

Many research reports are available on electrochemical properties of Li_2TiO_3. In prior work, Chauvaut et Cassir reported the Li^+ insertion as a diffusive process with the Ti non-stoichiometry in $Li_{2+x}Ti^{IV}_{1-x}Ti^{III}_xO_3$.[17] Wang et al.[18] studied the galvanostatic discharge-charge of an electrode Li_2TiO_3: acetylene black: PVDF binder (80:10:10) cycled at current rate of 0.5C, which showed a specific discharge capacity of 30 mAh g^{-1}. This value is comparable with 10 mAh g^{-1} reported by Tabuchi et al.[19] and 47 mAh g^{-1}reported by Morales et al.[20] for materials employed as anodes in non-aqueous rechargeable coin-type Li^+-ion cells. Close examination of these works shows that the electrochemical performance of Li_2TiO_3 is very sensitive to the morphology and size of particles induced by different synthesis process. In this context, β-Li_2TiO_3 has been considered as an element of composite electrodes, owing to its excellent structural stability and its good ionic conductivity with three-dimensional path for Li^+ ion migration. This phase was then used to enhance the electrochemical performance of various electrodes taking advantage of the strong Ti-O bond in Li_2TiO_3.[14,21-25] For example, in Si/Li_2TiO_3 nanocomposite synthesized by sol-gel method, Li_2TiO_3 acts as excellent buffer to the Si powders and partly compensate the capacity loss of the anode exhibiting a specific capacity of 471 mAh g^{-1} after 50 cycles.[25] The specific reversible capacity of Li_2TiO_3 was estimated to 100 mAh g^{-1}. The best results to our knowledge, were obtained with β-Li_2TiO_3, acetylene black as conductive agent and polyvinylidine fluoride (PVDF) binder at a weight ratio of 80:10:10, which delivered a capacity of 120 mAh g^{-1} at C/50 rate.[26]

In the present study, nanocrystalline Li_2TiO_3 and its composites Li_2TiO_3/graphene (denoted as LTO/Gr) and Li_2TiO_3/carbon nanotubes (denoted as LTO/CNTs) were synthesized by a simple solid-state reaction using commercially available carbon nanotubes and graphene sheets prepared via a thermal exfoliation route of oxidized graphite. The composites are investigated as anode materials for lithium-ion batteries using cyclic voltammetry, galvanostatic discharge-charge and cycling tests. These novel composites compared with Li_2TiO_3 show lower

impedance, high capacity and good structural stability with better cycleability than that of the pristine.

Experimental Section

Synthesis procedure

Li_2TiO_3 was synthesized by a solid-state reaction method using TiO_2 (anatase) and Li_2CO_3 taken as starting materials in stoichiometric ratio and then mixed in acetone and ball-milled for 24 h. The obtained precursor slurry was treated at 80 °C to obtain powders further calcinated at 800 °C for 12 h in Ar atmosphere. The Li_2TiO_3/graphene composite (denoted LTO/Gr) was prepared by the same method using 6 wt.% home-made graphene nanosheets. Li_2TiO_3/CNTs composite was synthesized using commercial TiO_2, Li_2CO_3 and CNTs provided by the University of Hyderabad as follows. The CNTs are multiwalled nanotubes with a diameter and length of about 20–30 nm and 1–2 μm, respectively. Firstly, TiO_2 and Li_2CO_3 were mixed in acetone and ball-milled for 24 h to obtain a homogeneous mixed slurry. In the second step, 6 wt.% CNTs were dispersed in acetone with sufficient ultrasonication to form a uniform slurry. Finally, the slurries were mixed together and treated at 80 °C. To obtain the Li_2TiO_3/CNTs nanocomposite, it was further calcinated at 800 ^oC for 12 h.

The two-dimensional graphene sheets have been prepared via a thermal exfoliation route, including graphite oxidation as an important step under modified Hummer method, followed by subsequent rapid thermal expansion of graphene oxide at 1050 °C in nitrogen atmosphere.[27] TiO_2 (anatase) and glucose were taken as starting materials with a weight ratio of 4:1 then mixed in ethanol–water compounds (10:1 in volume) and stirred for 2 h, further drying for 10 h under air-circulating oven at 100 °C. The obtained mixture was heated at 600 °C for 5 h under N_2 atmosphere to obtain carbon-coated TiO_2. The carbon content was 6 wt.%. Li_2CO_3, TiO_2 and graphene were dispersed in hexamethylene, and ball-milled under atmosphere at rotational speed of 200 rpm for 4 h. Finally, the LTO/Gr composite was obtained by drying the slurries at 80 °C and further calcination at 800 °C for 12 h in N_2 atmosphere.

Characterization

The sample structure was characterized by X–ray diffractometry (apparatus Siefert, model 3003 TT) using a CuKα radiation (λ =0.15406 nm). Data were collected in the 2θ range 10°–70°. The morphology and phase identification of the composites were observed using high resolution transition electron microscope (HRTEM) and selected-area electron diffraction using a HRTEM-FEI microscope (TECHNAI G^2 -30 S-twin D905) at an accelerating voltage of 200 kV. Field emission scanning electron microscopy (FE-SEM) was used to analyze the size and surface morphology of the particles with a SIRION 200 microscope. Raman scattering (RS) spectra were recorded at room temperature in the range of 200-3000 cm^{-1} using a Jobin–Yvon LAB RAM HR spectrometer with a spectral resolution of 1 cm^{-1}. The laser excitation source of 532 nm was produced by a air–cooled Nd:YAG laser doubled frequency at an excitation power of 50 mW. A 100× objective lens was used to focus the laser light on sample surface and the Raman spectra consisted of 20 acquisitions averaged together, with the duration of each acquisition set at 60 s.

Electrochemical tests

Electrochemical properties of the synthesized composites were investigated at room temperature using a three-electrode Pt//Li_2TiO_3 aqueous cell using the Li_2TiO_3 composite, an Ag/AgCl and a platinum metal strip as the working, reference and counter electrodes, respectively. The working electrode consisted of a mixture of 90 wt.% Li_2TiO_3/graphene, Li_2TiO_3/CNTs composite and 10 wt.% polyvinylidene fluoride (PVDF) dissolved in NMP (N-methyl-pyrrolidinone) to form a slurry spread on Ni metal substrate. This electrode of area of 0.25 cm^2 containing 3-4 μg of slurry was dried at 100 °C for 3 h to reduce impurity traces. The electrolyte was composed of 1 mol L^{-1} Li_2SO_4 in aqueous solution. The electrochemical performances were tested with an electrochemical workstation model CHI 608C (CH Instruments Inc., USA) in the potential range 0.0-1.0 V. Electrochemical impedance spectroscopy (EIS) was carried using a phase sensitive multimeter (model PSM 1700, UK) in the frequency range 1 Hz–1 MHz using a voltage bias of 5 mV.

Results and discussion

Structural properties

The X-ray diffraction patterns of pristine Li_2TiO_3, LTO/CNTs and Li_2TiO_3/Gr composite synthesized by solid-state reaction at 800 °C for 5 h are shown in Fig. 1. All XRD spectra exhibit the predominant (002) reflection line along with (110), (-131), (-133), (-204), (006), (312) and (062) characteristic peaks originated at 2θ values 18.48°, 20.22°, 35.68°, 47.47°, 57.35° and 62.96° corresponding to the monoclinic β-Li_2TiO_3 phase with *C*2/*c* space group (JCPDS No: 33-0831). The lattice parameters calculated by least-square fitting using eight Bragg lines *a*=5.069(1) Å, *b*=8.799(1) Å, *c*= 9.759(2) Å and β=100.2° are consistent with values of literature.[28,29] The elementary unit volume (*V*=*abc* sinβ) is 429.1 Å^3.

The addition of either graphene sheets or CNTs to the precursor does not influence the formation of the phase pure monoclinic Li_2TiO_3 during the heat treatment excepted a weak peak at 2θ = 26° marked by a star in the pattern of Li_2TiO_3/graphene composite (Fig. 1), which is due to re-stacking of graphene sheets in the disordered composite.[30] Note however that the intensity of this peak is very small, which means that the re-stacking is only marginal. The low intensity of the XRD peaks of the LTO/Gr composite is due to the screening of the LTO reflection by the presence of graphene. These results reveal that graphene and CNTs as carbonaceous additives do not have significant impact on the crystal structure of monoclinic Li_2TiO_3 prepared by solid-state reaction. Note that similar results were observed in the XRD patterns of Li*M*O/C composites (*M* = transition metal, C=carbonaceous material).[31,32] The crystallite size L_c of composites was calculated using the Scherrer's formula by considering the (002) reflection line:

$$L_c = \frac{K\lambda}{\beta \sin\theta}, \qquad (1)$$

where *K* is the Scherrer constant (0.89 for spherical crystallites), λ is the wavelength of X–ray radiation (0.15406 nm), β the full-width at half maximum (FWHM) expressed in radians and θ the Bragg angle. Values of the average crystallite size and lattice strain are listed in Table 1. The effect of carbon addition on LTO is the reduction of the crystallite size and the minimization of the lattice strain. The slowing-down of the crystallite growth rate of inorganic substances in presence of carbon in the synthesis process is well known.[33,34] The difference between the

crystallite size of composites and that of pristine LTO can be attributed to the fact that the great adsorbability and amorphous-like layer of active carbon retard the crystallite growth of Li_2TiO_3.

Table 1. Crystallite size and lattice train of LTO-based compounds.

Electrode material	Crystallite size (nm)	Lattice strain
Li_2TiO_3	38 ± 1	0.0105
Li_2TiO_3/graphene	29 ± 1	0.0032
Li_2TiO_3/CNTs	32 ± 1	0.0040

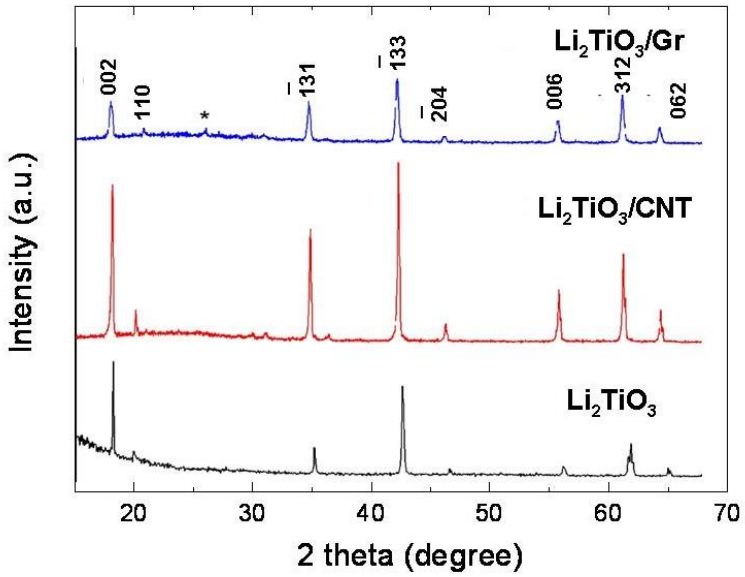

Figure 1. X–ray diffraction patterns of Li_2TiO_3, Li_2TiO_3/CNT and Li_2TiO_3/graphene samples. The reflection noted (*) is due to carbon.

The Raman spectra of pristine LTO, LTO/Gr and LTO/CNT recorded in the frequency range 200-3000 cm^{-1} are presented in Fig. 2. These spectra are composed of two contributions: the internal vibrations of the monoclinic LTO phase located in low-wavenumber region of 200-700 cm^{-1} and the spectral contribution of the carbon in the range 1200-3000 cm^{-1}. The spectrum of

Li_2TiO_3 contains three major vibrational modes situated at 666, 411 and 358 cm^{-1}, which are fingerprints of monoclinic structure. The strong band at 666 cm^{-1} is assigned to Ti–O stretching vibration of TiO_6 octahedra. The O-Ti–O bending vibrations are observed in the low-frequency region of 300-350 cm^{-1}. As Li ions occupy both octahedral and tetrahedral positions in Li_2TiO_3,[35] the vibrational mode observed at 411 cm^{-1} is attributed to Li–O stretching vibration in LiO_4 tetrahedra, while the weak band at 283 cm^{-1} is associated to Li–O bending vibration of LiO_6 octahedra.[36] The main feature of LTO/Gr and LTO/CNTs is the broadening of the Raman bands with respect to the LTO spectrum. Since the penetration depth of the laser beam in Raman experiments is small, Raman spectroscopy is a probe of the vibrations of molecular units in the vicinity of the surface of LTO in contact with the carbon. This is at contrast with XRD spectra that probe the core region of the LTO particles, because for particle size the order of 50 nm, the proportion of atoms in the surface layer is small. Therefore, the fact that the XRD spectra is not sensitive to the Gr and CNT means that the bulk of the particles is unaffected by the carbon, while the broadening of the Raman bands gives evidence that the bonds between the Li, O and Ti are affected at the surface in presence of the carbon. Therefore, these Raman spectra give evidence of a strong anchoring of the LTO particles on the carbon nanotubes or the graphene sheets. Such an effect has been observed with TiO_2 particles that disperse homogeneously on graphene sheets in presence of surface hydroxyl centers, due to the anchoring of the particles on the graphene sheets via esterification between hydroxyl groups of TiO_2 and carboxylic groups of graphene.[37,38] In the same way, this anchoring of the LTO particles on graphene evidenced by the band broadening in Fig. 2 explains why the LTO particles did not agglomerate, despite the propensity of titanate oxide particles to aggregate. This is a marked difference with the case when only acetylene black is simply added to the LTO particles, in which case the particles form agglomerates and the Raman bands are narrow,[26] meaning that there is no interaction between LTO and the acetylene black.

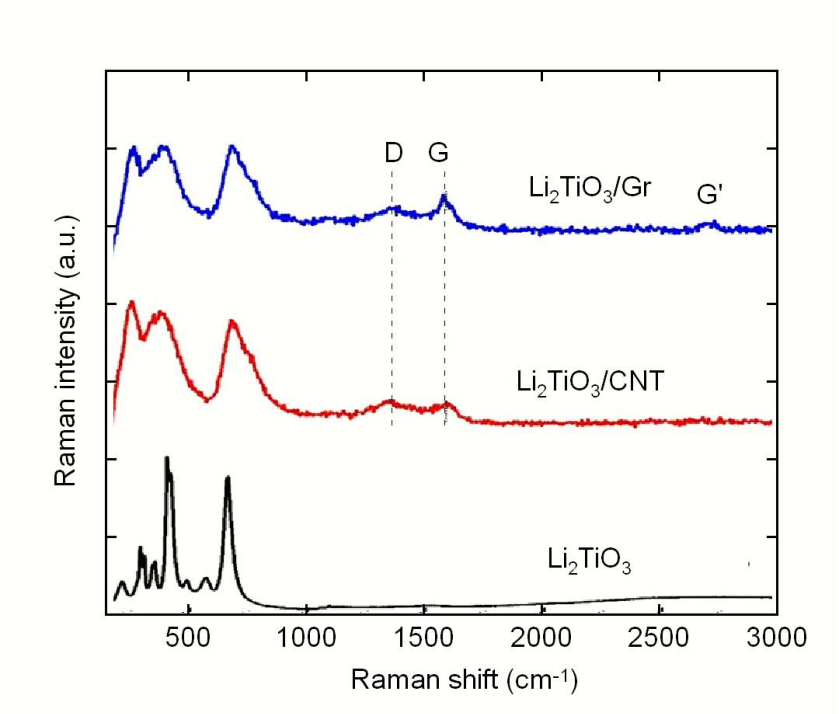

Figure 2. Raman scattering spectra of Li_2TiO_3, Li_2TiO_3/CNT and Li_2TiO_3/graphene samples. RS spectra were recorded using the 532 nm laser line as excitation source.

Three main Raman active modes of carbon ascribed to D–band, graphitic G–band and G'-band are observed at ~1347, ~1584, ~2690 cm^{-1}, respectively. The D band is the so-called "disordered induced band" attributed to the vibration of carbon lattice disturbed by edges/defects (*K*-point phonons with A_{1g} symmetry), the graphitic G–band is the primary in–plane breathing mode of hexagonal sp^2-carbon rings of graphite (E_{2g} phonons) and the G' band is a second-order overtone of a different in-plane vibration of D-band. These spectral features can be applied to both graphene and CNTs materials.[39] The Raman intensity of the D band increases with increasing the amount of disorder in graphene. Thus, the ratio of the absolute peak intensities I_D/I_G indicates the degree of graphitization of composites.[40,41] The value of I_D/I_G for both LTO/Gr and LTO/CNTs is ~0.5 and ~1.0, respectively, suggesting that the degree of graphitization of carbon in graphene is higher than that in CNTs sample; this implies a higher electrical conductivity and an increase of the rate capability of the LTO/Gr electrode.[10]

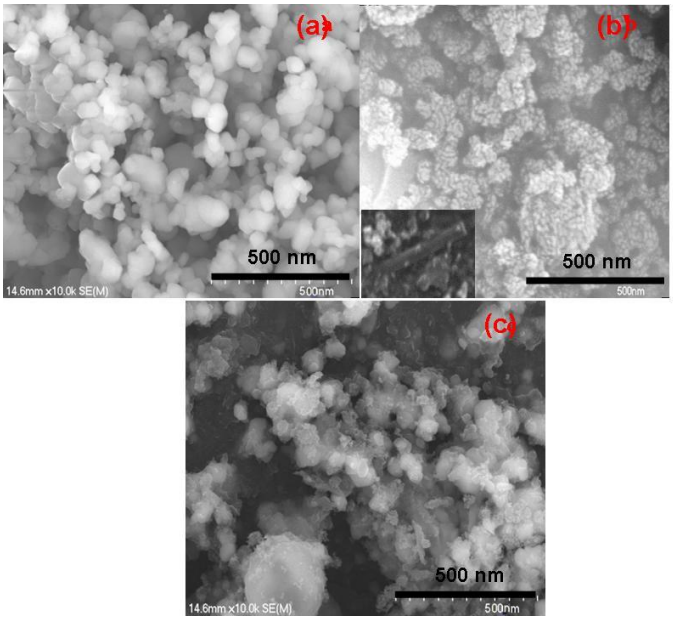

Figure 3. SEM images of (a) Li_2TiO_3, (b) Li_2TiO_3/CNT and (c) Li_2TiO_3/graphene samples.

The morphology and microstructure of pristine LTO and its composites were studied from FE-SEM and TEM experiments. Figure 3 presents the SEM images of the three samples, which obviously show smaller particles (~50-70 nm) for LTO/Gr and LTO/CNTs composites than for pristine Li_2TiO_3 (~100-150 nm). This observation matches well with the crystallite data from XRD. As particle sizes are comparable to those of crystallite sizes deduced from Eq. 1, we conclude that LTO particles are mainly single crystals. They are homogeneously distributed and have a monoclinic-like shape with well-defined facets (Fig. 3a). Figure 3b-c depicts the SEM images of LTO/CNT and LTO/Gr composites, respectively. These images confirm the smaller grain sizes for LTO particles grown in the presence of carbon. The CNTs are wrapped into all the Li_2TiO_3 particles, indicating that well-connected CNTs adhere closely on the surface of the Li_2TiO_3 particles and form a conductive network. This network provides strong anchoring between Li_2TiO_3 nanoparticles, facilitating fast electronic transport that results in a significant improvement in rate capability of the electrode material. The LTO/CNTs composite particles are also well distributed with a tendency to agglomerate. In the SEM image of LTO/Gr composite (Fig. 3c), the LTO particles are well-dispersed among the graphene sheets, which extend in all directions like a stretched network.

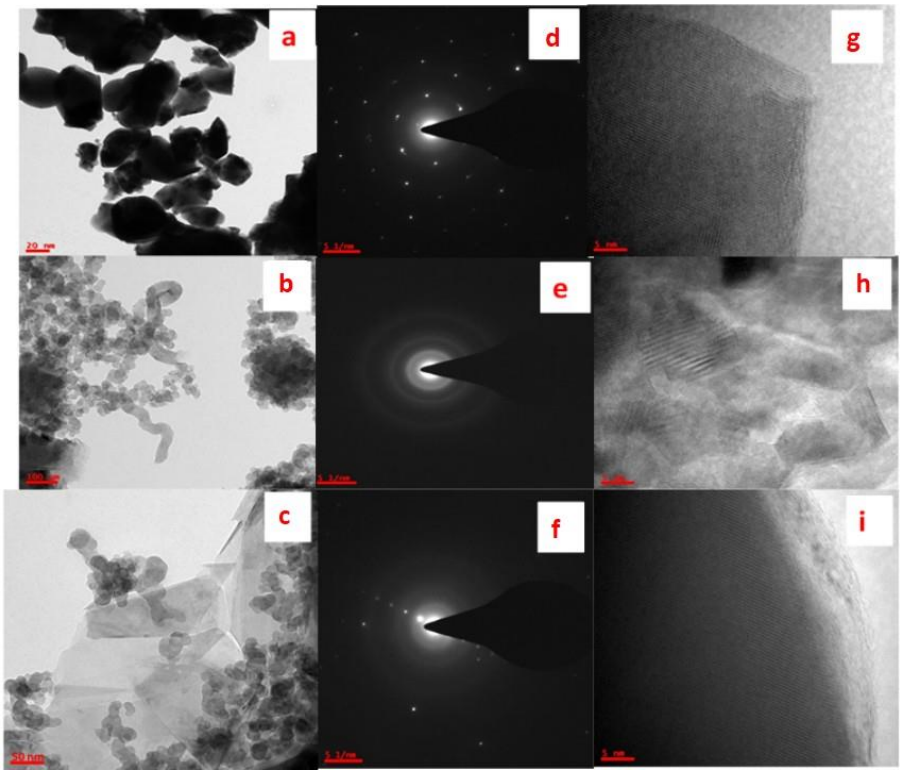

Figure 4. TEM, HRTEM images and SAED patterns of Li_2TiO_3, Li_2TiO_3/CNT, and Li_2TiO_3/graphene samples. (a-c) low magnification TEM images, (d-f) SAED patterns and (g-i) HRTEM images.

Figures 4a-c show the detailed microstructure of LTO observed by TEM and SAED micrographs. The low-magnification TEM bright field image (Fig. 4a) shows well-dispersed particles with relatively uniform nanostructured shape. Figure 4b displays the SAED pattern of LTO, which clearly presents bright spots; the observation of (002), (-131) and (-133) diffraction spots indicates a high crystallinity of the material. The HRTEM image (Fig. 4c) confirms the well-resolved lattice of pristine LTO with fringes at interplanar distance ~0.47 nm corresponding to the (002) plane. Figure 4d presents the SAED pattern of the LTO/CNTs composite, which displays blurred diffraction rings indicating the nanosized carbon particles that are wrapped on LTO grains. Similar pattern with blurred rings is observed for the LTO/Gr composite. The TEM image of the LTO/Gr composite is shown in Fig. 4e, in which well-dispersed graphene

nanosheets connect the LTO particles and form a conducting network with a robust inner connected architecture. Figure 4f depicts the HRTEM image of LTO/Gr composite; it gives clear evidence that graphene sheets stick on LTO particles as a 3-5-nm thick pseudo-coating deposited on the surface (graphene layer). The LTO/Gr composite obtained by an annealing step of the LTO precursor at 800 °C reveals a unique morphology of submicron-sized particles. This temperature is commonly used for the carbonization process of electrode materials, for examples $LiFePO_4$,[40] and $Li_4Ti_5O_{12}$,[42] for which a ~5-nm thick carbon layer favors their high electrochemical performance.

Electrochemical properties

Figure 5 shows the cyclic voltammograms (CV) of aqueous cells with LTO, LTO/CNTs and LTO/Gr composites carried out in the voltage range 0.0 -1.0 V at 1 mV s^{-1} sweep rate using 1 mol L^{-1} saturated Li_2SO_4 electrolyte. These CV curves are similar for all electrodes indicating that the addition of ~6 wt.% of graphene and CNTs does not affect the electrochemical redox response of the LTO active material. One set of well–defined oxidation/reduction peaks is observed at 0.64/0.29 V for LTO/graphene, 0.75/0.22 V for LTO/CNT, 0.8/0.2 V vs. Li^+/Li^0 for pristine LTO. which are attributed to the redox reaction of Ti^{4+}/Ti^{3+} related to the reduction of Ti^{IV} upon the insertion of a fraction x of Li^+ ions. The CV current peaks for composites are stronger than those of pristine Li_2TiO_3 electrodes, which gives evidence of an improvement of electron transport and enhancement of the lithium-ion diffusion in composite frameworks. The potential separation between the oxidation and reduction peaks (ΔE_p) appearing in the order ΔE_p(LTO/Gr) < ΔE_p(LTO/CNTs < ΔE_p(LTO) indicates the decreasing degree of polarization of the LTO/Gr electrode due to the higher electronic conductivity of the unique integrated architecture with graphene. The graphene nanosheets facilitate the 3D network that well electrically connects the LTO particles to the current collector. As a consequence, $Li_4Ti_5O_{12}$/graphene composite as anode material delivered 96% of its initial capacity after 50 cycles at 10C rate.[43]

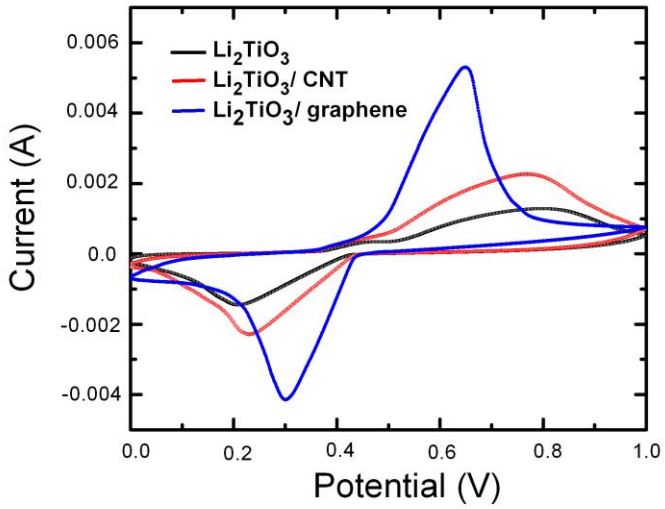

Figure 5. Cyclic voltammograms carried out at 1 mV s^{-1} sweep rate for lithium cells including Li_2TiO_3, Li_2TiO_3/CNT, Li_2TiO_3/graphene as anode materials.

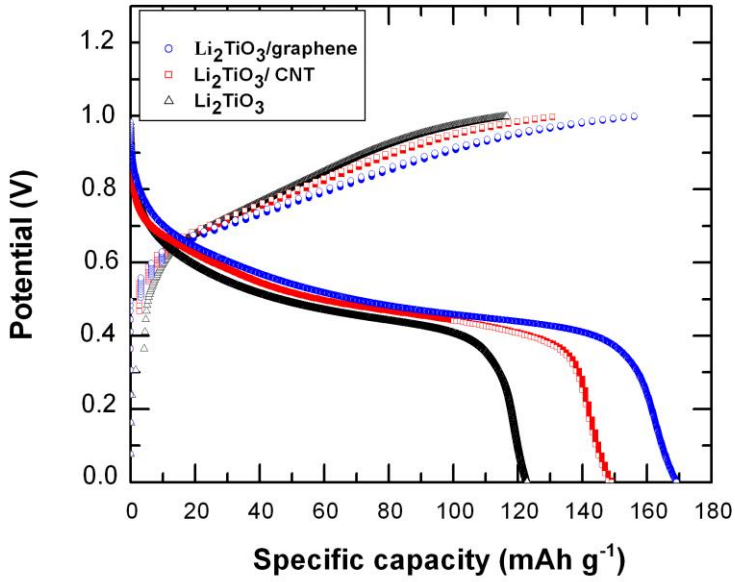

Figure 6. Charge-discharge curves performed at 1C rate of lithium cells including Li_2TiO_3, Li_2TiO_3/CNT, Li_2TiO_3/graphene as anode materials.

Figure 6 shows the discharge-charge curves of the aqueous lithium cells with LTO-based electrodes. Galvanostatic measurements were carried out in the cutoff voltage 0.0 -1.0 V at 1C rate. The S-shape of the charge-discharge profiles of the Li//Li_2TiO_3 cell with a mid-voltage of ~0.5 V corresponds to the formation of a non-stoichiometric single phase $Li_{2+x}TiO_3$ without formation of distinct plateaus. Similar electrochemical behavior is noticed for Li//Li_2TiO_3/Gr and Li//Li_2TiO_3/CNTs cells. Initial specific discharge capacities of 149 and 154 mAh g^{-1} are respectively delivered in the first cycle by LTO/CNTs and LTO/Gr composite electrodes against 122 mAh g^{-1} for the pristine electrode (the theoretical capacity of LTO being 229 mAh g^{-1}). Note that electrodes using composite materials do not have additive carbon such carbon Super-P or acetylene black, so that the use of only 6 wt.% of graphene or CNTs is a gain of gravimetric capacity of the whole cell. Both CV and galvanostatic results match well, showing the best electrochemical performance of the LTO/Gr composite because of the high efficiency of the conductive network among the LTO nanoparticles. Note that the electrochemical features of Li_2TiO_3 are different from the behaviors of $Li_4Ti_5O_{12}$ spinel, which displays a wide voltage plateau at 1.5 V upon insertion of 3Li per formula unit.[44]

Electrochemical impedance spectroscopy (EIS) was carried out over the frequency range from 1 Hz to 1 MHz for electrodes in the fully charged state. Figure 7 depicts the Nyquist diagrams (EIS curves) of Li_2TiO_3/graphene, Li_2TiO_3/CNT composite and pristine Li_2TiO_3. Nyquist plots are composed of three contribution: (1) the interception of *x*–axis at high frequency indicates the solution resistance or ohmic resistance (R_s) contributed by electrolyte, (2) the depressed semicircle in the high- and intermediate-frequency range originates from the charge transfer resistance R_{ct} corresponding to solid-state diffusion of Li^+ in the bulk of the active material and the contact phase angle element (CPE) including double layer capacitance,[45] and (3) further, at the low-frequency region, a straight line is ascribed to the Warburg impedance corresponding to the diffusion regime of Li^+ ions through the LTO electrode. As shown in Fig. 7, the depressed semicircle of LTO/Gr composite is smaller than those of other samples that implies higher electronic and ionic conductivity. The impedance spectra were fitted using the Randles equivalent circuit shown in the inset of Fig. 7. Calculated values of ohmic resistance R_S, charge

transfer resistance R_{ct} are listed in Table 2. The smaller charge transfer resistance of LTO/Gr, i.e. 93 Ω vs. 180 Ω for LTO/CNTs is consistent with the previous electrochemical data. The Warburg regime observed at low frequencies gives evidence that the insertion mechanism of Li^+ ions into the LTO-based electrode is strongly controlled by a diffusion process. In this regime, the impedance varies with the angular frequency ω according to the law:[46]

$$Z' = R_s + R_{ct} + \sigma_w \omega^{-1/2}, \quad (2)$$

The Warburg impedance σ_w is obtained from the slope of Z' vs. $\omega^{-1/2}$ in the low-frequency range (Fig. 8). Typical values of σ_w are listed in Table 2. EIS can be used to evaluate the apparent Li-ion diffusion coefficient D_{Li+} from the low-frequency Warburg impedance according the equation:[46]

$$D_{Li^+} = \frac{1}{2}\left[\frac{RT}{F^2 A C_{Li} \sigma_w}\right]^2, \quad (3)$$

where R, T and F are the usual constants, A the surface area of the electrode-electrolyte interface, C_{Li} is the lithium-ion concentration in the electrode. Values of D_{Li+} are reported in Table 2. We observed an increase of D_{Li+} by a factor 2 for the LTO/Gr sample. The high values of the diffusion coefficient of Li+ ions ($D_{Li+} > 10^{-9}$ cm^2 s^{-1}) reflect the ionic character of Li_2TiO_3 materials. Therefore, the composite LTO/Gr has the lower Warburg factor σ_w, which results in its higher $D_{Li+} = 1.1\times10^{-8}$ cm^2 s^{-1}.

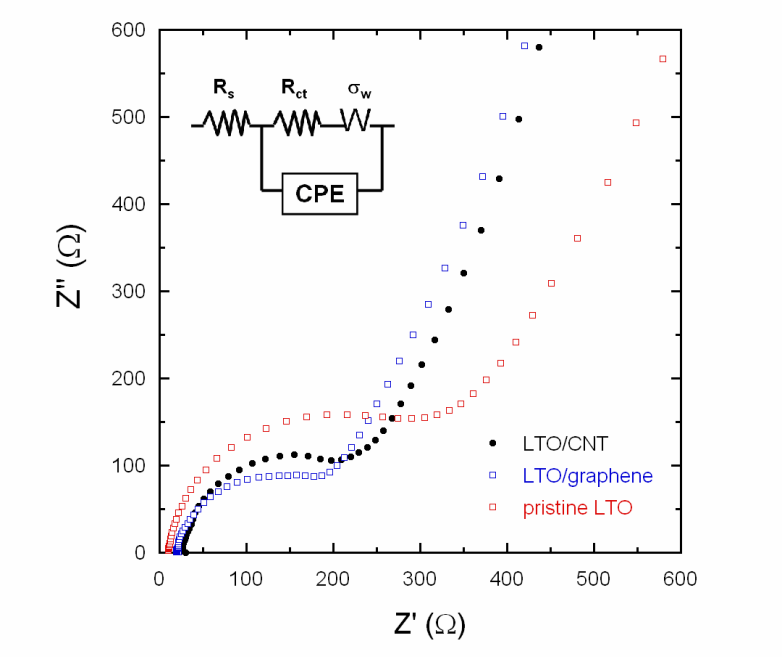

Figure 7. Electrochemical impedance spectra of Li_2TiO_3, Li_2TiO_3/ CNT, Li_2TiO_3/graphene anode materials.

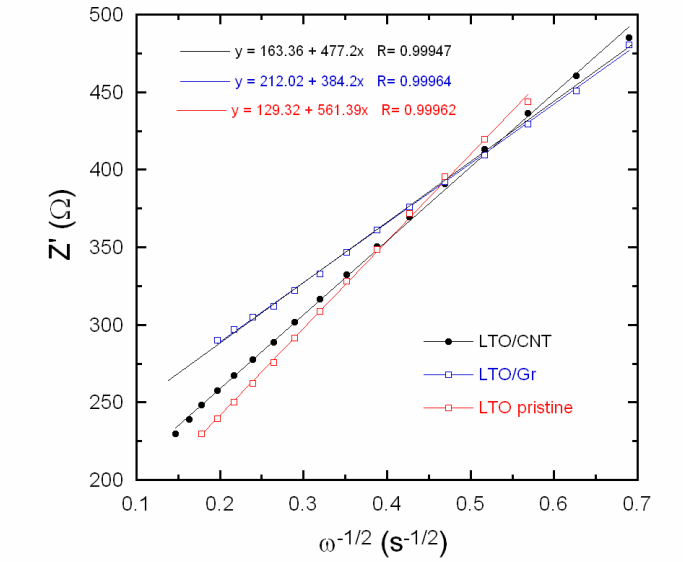

Figure 8. Z' vs. $\omega^{-1/2}$ plots in the Warburg region of the impedance spectra for Li_2TiO_3, Li_2TiO_3/ CNT, Li_2TiO_3/graphene samples.

Table 2. Results of the EIS measurements. Fitting was performed using the Randles equivalent circuit shown in the insert of Fig. 7.

Electrode	R_s (Ω)	R_{ct} (Ω)	Z_w (Ω $s^{-1/2}$)	D_{Li+} (cm^2 s^{-1})
LTO	12	244	561	5.2×10^{-9}
LTO/Gr	19	93	384	1.1×10^{-8}
LTO/CNT	19	180	477	6.1×10^{-9}

Figure 9 shows the cycleability of the LTO-based electrodes for lithium cells cycled at discharging and charging constant current of 1C rate. All the electrodes have good electrochemical stability. The initial discharge capacity of LTO/Gr, LTO/CNTs and LTO still remained at 150, 143 and 113 mAh g^{-1} respectively, even after 30 discharge cycles. The LTO/Gr composite exhibits the best cycling performance with capacity retention of 98% compared to 93% for LTO. In summary, among the LTO-based electrode, the results reveal that the LTO/Gr composite exhibits the best cycling stability and rate capability.

This capacity of 150 mAh g^{-1} at high current density (1C rate) is due to different synergetic effects. First, the high electrical conductivity of the graphene improves the rate capability. Second, the anchoring of the LTO particles on the graphene sheets, prevents the re-stacking of the graphene sheets despite the high sintering temperature in the synthesis process. Third, this anchoring also insures a homogeneous distribution of LTO particles on the graphene sheets. As a consequence, LTO/Gr is thus composite that allows LTO to deliver the best capacity that has been reported for this material so far in the literature, to our knowledge.

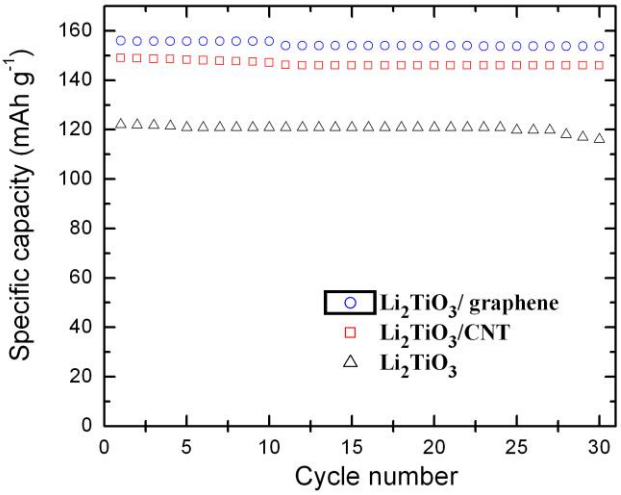

Figure 9. Cycling performance for Li_2TiO_3, Li_2TiO_3/ CNT and Li_2TiO_3/ graphene anode materials discharged at 1C rate.

Conclusions

The nanocomposites Li_2TiO_3/graphene and Li_2TiO_3/carbon nanotubes synthesized by a simple solid-state reaction for use as superior lithium storage electrodes. The structure, morphology and electrochemical properties of these electrodes have been investigated by X-ray diffraction, Raman spectroscopy, FE-SEM and TEM, cyclic voltammetry and galvanostatic discharge-charge. The homogenous and stable structures afford a highly conductive matrix for Li-ion insertion to LTO nanoparticles and reduces the lithium ion and electron transport diffusion resistances. The graphene and CNTs provide conductive network among the LTO nanoparticles that improves the rate capability and cycleability of anodes. The discharge capacity of 154 and 149 $mAhg^{-1}$ at 1C rate and the capacity retention of 98 % and 96% after 30 cycles have been evaluated for LTO/Gr and LTO/CNTs electrodes, respectively.

Conflicts of interest

There are no conflicts to declare

References

[1] C.M. Julien, A. Mauger, A. Vijh, K. Zaghib, Lithium Batteries: Science and Technology, Springer, Heidelberg, 2016.

[2] L. Lu, X. Han, J. Li, J. Hua, M. Ouyang, A review on the key issues for lithium-ion battery management in electric vehicles. *J. Power Sources* **2013**, 226, 272-288.

[3] A. Mauger, C. Julien, Critical review on lithium-ion batteries: are they safe? Sustainable? *Ionics* **2017**, 23, 1933-1947.

[4] Y. Li, G.L. Pan, J.W. Liu, X.P. Gao, Preparation of $Li_4Ti_5O_{12}$ nanorods as anode materials for lithium-ion batteries. *J. Electrochem. Soc*., 2009, 156, A495–A499.

[5] A. Laumann, K.T. Fehr, M. Wachsmann, M. Holzapfel, B.B. Iversen, Metastable formation of low temperature cubic Li_2TiO_3 under hydrothermal conditions — Its stability and structural properties. *Solid State Ionics*, 2010, 181, 1525–1529.

[6] U. Dash, S. Sahoo, P. Chaudhuri, S.K.S. Parashar, K. Parashar, Electrical properties of bulk and nano Li_2TiO_3 ceramics: a comparative study. *J. Adv. Ceram*., 2014, 3, 89-97.

[7] J.-S. Kim, C.S. Johnson, J.T. Vaughey, M.M. Thackeray, S.A. Hackney, W. Yoon, C.P. Grey, Electrochemical and structural properties of $xLi_2M'O_3 \cdot (1-x)LiMn_{0.5}Ni_{0.5}O_2$ electrodes for lithium batteries (M'=Ti, Mn, Zr; $0 \leq x \leq 0.3$). *Chem. Mater*., 2004, 16, 1996-2006.

[8] J.S. Park, S.-H. Baek, Y.-I. Jeong, B.-Y. Noh, J.H. Kim, Effects of a dopant on the electrochemical properties of $Li_4Ti_5O_{12}$ as a lithium-ion battery anode material. *J. Power Sources*, 2013, 244, 527–531.

[9] Y. Li, G.L. Pan, J.W. Liu, X.P. Gao, Preparation of $Li_4Ti_5O_{12}$ nanorods as anode materials for lithium-ion batteries. J. Electrochem. Soc., 156 (2009) A495–A499.

[10] P. Zhang, M. Chen, X. Shen, Q. Wu, X. Zhang, L. Huan, G. Diao, Preparation of $Li_4Ti_5O_{12}$ nanosheets/carbon nanotubes composites and application of anode materials for lithium-ion batteries. Electrochim. Acta, 204 (2016) 92–99.

[11] Z. Zhang, L. Cao, J. Huang, S. Zhou, Y. Huang, Y. Cai, Hydrothermal synthesis of Zn-doped $Li_4Ti_5O_{12}$ with improved high rate properties for lithium ion batteries. *Ceram. Int*., 2013, 39, 6139–6143.

[12] Y.-G. Guo, Y.-S. Hu, W. Sigle, J. Maier, Superior electrode performance of nanostructured mesoporous TiO_2 (anatase) through efficient hierarchical mixed conducting networks. *Adv. Mater*., 2007, 19, 2087-2091.

[13] Y. Ren, P. Lu, X. Huang, S. Zhou, Y. Chen, B. Liu, F. Chu, J. Ding, In-situ synthesis of nano-$Li_4Ti_5O_{12}$/C composite as an anode material for Li-ion batteries. *Solid State Ionics*, 2015, 274, 83–87.

[14] Y.N. Ko, S.H. Choi, Y.C. Kang, S.B. Park, Characteristics of Li_2TiO_3-$LiCrO_2$ composite cathode powders prepared by ultrasonic spray pyrolysis. *J. Power Sources*, 2013, 244, 336-343.

[15] Y. Chen, H. Zhang, Y. Li, Y. Chen, T. Luo, Electrochemical performance of $Li_4Ti_5O_{12}$/carbon nanotubes/graphene composite as an anode material in lithium-ion batteries. *Int. J. Hydrogen Energy*, 2017, 42, 7195-7201.

[16] J. Shu, L Hou, R Ma, M Shui, L Shao, D Wang, Y Ren, W Zheng. In situ fabrication of $Li_4Ti_5O_{12}$@CNT composites and their superior lithium storage properties. *RSC Adv*., 2012, 2, 10306–10309.

[17] V. Chauvaut, M. Cassir, Electrochemical intercalation of Li^+ in Li_2TiO_3 at 600 and 650 °C. *J. Electroanal. Chem*., 1999, 474, 9-15.

[18] Y. Wang, A. Zhou, X. Dai, L. Feng, J. Li, Solid-state synthesis of submicron-sized $Li_4Ti_5O_{12}$/Li_2TiO_3 composites with rich grain boundaries for lithium ion batteries. *J. Power Sources*, 2014, 266, 114-120.

[19] M. Tabuchi, A. Nakashima, H. Shigemura, K. Ado, H. Kobayashi, H. Sakaebe, K. Tatsumi, H. Kageyama, T. Nakamura, R. Kanno, Fine $Li_{(4-x)/3}Ti_{(2-2x)/3}Fe_xO_2$ ($0.18 \leq x \leq 0.67$) powder with cubic rock-salt structure as a positive electrode material for rechargeable lithium batteries. *J. Mater. Chem*., 2003, 13, 1747-1757.

[20] J. Morales, J. Santos-Pena, R. Trocoli, S. Franger, Electrochemical activity of rock-salt-structured $LiFeO_2$-$Li_{4/3}Ti_{2/3}O_2$ nanocomposites in lithium cells. *J. Nanopart. Res*., 2008, 10, 217-226.

[21] H. Shigemura, M. Tabuchi, H. Sakaebe, H. Kobayashi, H. Kageyama, Lithium extraction and insertion behavior of nanocrystalline Li_2TiO_3-$LiFeO_2$ solid solution with cubic rock salt structure. *J. Electrochem. Soc*., 150 (2003) A638-A644.

[22] L. Zhang, X. Wang, H. Noguchi, M. Yoshio, K. Takada, T. Sasaki, Electrochemical and ex situ XRD investigations on (1-x)$LiNiO_2$•xLi_2TiO_3 ($0.05 \leq x \leq 0.5$). *Electrochim. Acta*, 49 (2004) 3305-3311.

[23] X. Yang, R. Yu, L. Ge, D. Wang, Q. Zhao, X. Wang, Y. Bai, H. Yuan, H. Shu, Facile synthesis and performances of nanosized Li_2TiO_3-based shell encapsulated $LiMn_{1/3}Ni_{1/3}Co_{1/3}O_2$ microspheres. *J. Mater. Chem. A*, 2014, 2, 8362−8368.

[24] J. Shi, Y. Liang, L. Li, Y. Peng, H. Yang, Evaluation of the electrochemical characteristics of silicon/lithium titanate composite as anode material for lithium ion batteries. *Electrochim. Acta*, 2015, 155 125-131.

[25] H.S Bhatti, D. Anjum, S. Ullah, B. Ahmed, A. Habib, A. Karim, S.K. Hasanain, Electrochemical characteristics and Li ion intercalation kinetics of dual-phase $Li_4Ti_5O_{12}$/Li_2TiO_3 composite in voltage range of 0-3 V. *J. Phys. Chem. C,* 2016, 120, 9553-9561.

[26] A.L. Narayana, M. Dhananjaya, N.G. Prakash, O.M. Hussain, C. M. Julien, Nanocrystalline Li_2TiO_3 electrodes for supercapattery application. *Ionics*, 2017, 23, 3419–3428.

[27] H.C. Schniepp, J.L. Li, M.J. McAllister, H. Sai, M. Herrera-Alonso, D.H. Adamson, R.K. Prud'homme, R. Car, D.A. Saville, I.A. Aksay. *J. Phys. Chem. B,* 2006, 110, 8535-8539.

[28] J.F. Dorrian, R.E. Newnham, Refinement of the structure of Li_2TiO_3. *Mater. Res. Bull*., 1969, 4, 179-183.

[29] K. Kataoka, Y. Takahashi, N. Kijima, H. Nagai, J. Akimoto, Y. Idemoto, K.-I. Ohshima, Crystal growth and structure refinement of monoclinic Li_2TiO_3. *Mater. Res. Bull*., 2009, 44, 168–172.

[30] C. Yu, C.-F. Wang, S. Chen, Facile access to graphene oxide from ferro-induced oxidation. *Sci. Rep*., 2015, 6, 17071.

[31] O. Rosas, J. Saunders, H. Castaneda, Interfacial electrochemical analysis on $LiCoO_2$/carbon nanotubes layers as cathode composite in aqueous electrolytes. *Electrochim. Acta*, 2013, 113, 77-86.

[32] U. Dettlaff-Weglikowska, J. Yoshida, N. Sato, S. Roth, Effect of single-walled carbon nanotubes as conductive additives on the performance of $LiCoO_2$-based electrodes, J. Electrochem. Soc. 158 (2011) A174.

[33] S.R. Davis, A.V. Chadwick, J.D. Wright, The effects of crystallite growth and dopant migration on the carbon monoxide sensing characteristics of nanocrystalline tin oxide based sensor materials. *J. Mater. Chem*., 1998, 8, 2065-2071.

[34] Y.-J. Li, X.-D. Li, J.-W. Li, J. Yin, C.-X. Feng, Effects of active carbon carrier on phase transform and crystallite growth of titanium dioxide in TiO_2/AC. *J. Inorg. Mater*., 2005, 20, 291-298.

[35] R. Ramaraghavulu, S. Buddhudu, G. Bhaskar Kumar, Analysis of structural and thermal properties of Li_2TiO_3 ceramic powders. *Ceram. Int*., 2011, 37, 1245–1249.

[36] J.J. Bian, Y.F. Dong, Sintering behavior, microstructure and microwave dielectric properties of $Li_{2+x}TiO_3$ ($0 \leq x \leq 0.2$). *Mater. Sci. Eng. B*, 2011, 176, 147–151.

[37] C.-Y. Wu, K.-J. Tu, J.-P. Deng, Y.-S. Lo, C.-H. Wu, Markedly enhanced surface hydroxyl groups of TiO_2 nanoparticles with superior water-dispersibility for phtocatalysis. *Materials*, 2017, 10, 566.

[38] K. Zhang, K. C. Kemp, V. Chandra, Homogeneous anchoring of TiO_2 nanoparticles on graphene sheets for waste water treatment. *Mater. Lett*., 2012, 81, 127-130.

[39] L.M. Malard, M.A. Pimenta, G. Dresselhaus, M.S. Dresselhaus, Raman spectroscopy in graphene. *Phys. Rep*., 2009, 473, 51-87.

[40] C.M. Julien, K. Zaghib, A. Mauger, M. Massot, A. Ait-Salah, M. Selmane, F. Gendron, Characterization of the carbon coating onto $LiFePO_4$ particles used in lithium batteries. *J. Appl. Phys*., 2006, 100, 063511.

[41] A. Sadezky, H. Muckenhuber, H. Grothe, R. Niessner, U. Poschl, Raman microspectroscopy of soot and related carbonaceous materials: spectral analysis and structural information. *Carbon* 2005, 43, 1731-1742.

[42] X.F. Guo, C.Y. Wang, M.M. Chen, J.Z. Wang, J.M. Zheng, Carbon coating of $Li_4Ti_5O_{12}$ using amphiphilic carbonaceous material for improvement of lithium-ion battery performance. *J. Power Sources*, 2012, 214, 107-112.

[43] Q. Zhang, W. Peng, Z. Wang, X. Li, X. Xiong, H. Guo, Z.O. Wang, F.G. Wu, Synthesis and characterization of $Li_4Ti_5O_{12}$/graphene composite as anode material with enhanced electrochemical performance. *Ionics*, 2013, 19, 717–723.

[44] L. Aldon, P. Kubiak, M. Womes, J.C. Jumas, J. Olivier-Fourcade, J.L. Tirado, J.I. Corredor, C. Prez-Vicente, Chemical and electrochemical Li-insertion into the $Li_4Ti_5O_{12}$ spinel. *Chem. Mater*., 2004, 16, 5721-5725.

[45] K.M. Shaju, G.V. Subba-Rao, B.V.R. Chowdari, EIS and GITT studies on oxide cathodes, O2-$Li_{2/3+x}(Co_{0.15}Mn_{0.85})O_2$ (x=0 and 1/3). *Electrochim. Acta*, 2003, 48, 2691-2703.

[46] X. Zhang, A. Mauger, Q. Lu, H. Groult, L. Perrigaud, F. Gendron, CM. Julien, Synthesis and characterization of $LiNi_{1/3}Mn_{1/3}Co_{1/3}O_2$ by wet-chemical method. *Electrochim. Acta*, 2010, 55, 6440-6449.